Membrane Mobility and Microdomain Association of the Dopamine Transporter Studied with Fluorescence Correlation Spectroscopy and Fluorescence Recovery after Photobleaching†

Erika M. Adkins,‡ Devadoss J. Samuvel,§ Jacob U. Fog,‡ Jacob Eriksen,‡ Lankupalle D. Jayanthi,§ Christian Bjerggaard Vaegter,‡ Sammanda Ramamoorthy,*,§ and Ulrik Gether*,‡

Molecular Neuropharmacology Group, Department of Neuroscience and Pharmacology and Center for Pharmacogenomics, The Panum Institute, University of Copenhagen, DK-2200 Copenhagen, Denmark, and Department of Neurosciences, Division of Neuroscience Research, Medical University of South Carolina, Charleston, South Carolina 29425

Received March 3, 2007; Revised Manuscript Received June 14, 2007

ABSTRACT: To investigate microdomain association of the dopamine transporter (DAT), we employed FCS (fluorescence correlation spectroscopy) and FRAP (fluorescence recovery after photobleaching). In non-neuronal cells (HEK293), FCS measurements revealed for the YFP-DAT (DAT tagged with yellow fluorescent protein) a diffusion coefficient (*D*) of $\sim 3.6 \times 10^{-9}$ cm^2/s, consistent with a relatively freely diffusible protein. In neuronally derived cells (N2a), we were unable to perform FCS measurements on plasma membrane-associated protein due to photobleaching, suggesting partial immobilization. This was supported by FRAP measurements that revealed a lower *D* and a mobile fraction of the YFP-DAT in N2a cells compared to HEK293 cells. Comparison with the EGFP-EGFR (epidermal growth factor receptor) and the EGFP-β2AR (β2 adrenergic receptor) demonstrated that this observation was DAT specific. Both the cytoskeleton-disrupting agent cytochalasin D and the cholesterol-depleting agent methyl-β-cyclodextrin (mβCD) increased the lateral mobility of the YFP-DAT but not that of the EGFP-EGFR. The DAT associated in part with membrane raft markers both in the N2a cells and in rat striatal synaptosomes as assessed by sucrose density gradient centrifugation. Raft association was further confirmed in the N2a cells by cholera toxin B patching. It was, moreover, observed that cholesterol depletion, and thereby membrane raft disruption, decreased both the V_{max} and K_M values for [^{3}H]dopamine uptake without altering DAT surface expression. In summary, we propose that association of the DAT with lipid microdomains in the plasma membrane and/or the cytoskeleton serves to regulate both the lateral mobility of the transporter and its transport capacity.

The rapid removal of dopamine from the synaptic cleft is mediated by the presynaptically localized dopamine transporter (DAT)[1] that belongs to the SLC6 (solute carrier 6) gene family of Na^+/Cl^- coupled transporters (*1*−*3*). The DAT is closely related to the serotonin and norepinephrine transporters, and collectively, they make up the biogenic amine transporter subfamily (*1*−*3*). In addition to playing a critical role in the termination of biogenic amine signaling, the biogenic amine transporters are important pharmacological targets. The DAT is the primary target for widely abused psychoactive compounds, such as amphetamines and cocaine, whereas the SERT and NET are targets for antidepressant medicines (*1*−*3*). Recently, the structure of a bacterial homologue of the SLC6 carriers was determined at 1.65 Å resolution (*4*). On the basis of this structure, and the wealth of information obtained from mutagenesis studies (*5*, *6*), the biogenic amine transporters are believed to be oligomeric proteins composed of functionally separate protomers each containing 12 transmembrane segments in a fold unique to this class of transporters.

Similar to other membrane proteins, the biogenic amine transporters are predicted not to be randomly distributed in the plasma membrane but associated with intracellular protein networks and plasma membrane microdomains that ensure appropriate spatial and temporal regulation of transporter function in the presynaptic membrane. At present, little is known about the nature of these networks and microdomains. There is, however, a growing body of evidence of tight association between the biogenic amine transporters and larger regulatory protein complexes. For example, the DAT has been shown to bind the multiple-LIM-domain-containing adaptor protein HIC-5 (*7*), the SNARE protein syntaxin 1A

† This work was supported in part by the National Institutes of Health Grants P01 DA 12408 (U.G.), P50DA015369 (S.R.), and MH062612 (S.R.), the Lundbeck Foundation (U.G.), the Danish Health Science Research Council (U.G.), the Novo Nordisk Foundation (U.G.), the A. P. Moeller Foundation (U.G.), and the Carlsberg Foundation (E.M.A.).

* To whom correspondence should be addressed: Molecular Neuropharmacology Group, Department of Neuroscience and Pharmacology, The Panum Institute 18.6, University of Copenhagen, DK-2200 Copenhagen N, Denmark. Telephone: 45-3532-7548. Fax: 45-3532-7555. E-mail: gether@neuropharm.ku.dk.

‡ University of Copenhagen.

§ Medical University of South Carolina.

[1] Abbreviations: DAT, dopamine transporter; EGFP, enhanced green fluorescent protein; FCS, fluorescence correlation spectroscopy; FRAP, fluorescence recovery after photobleaching; mβCD, methyl-β-cyclodextrin; ROI, region of interest; YFP, yellow fluorescent protein; TfR, transferrrin receptor; CTB, cholera toxin B.

10.1021/bi700429z CCC: $37.00
Published on Web 08/22/2007

(*8*), the PDZ domain protein PICK1 (*9*, *10*), and Ca^{2+}/calmodulin-dependent protein kinase (*11*).

Membrane proteins, such as the biogenic amine transporters, might also be segregated into distinct plasma membrane domains with specific lipid compositions. These microdomains include so-called "lipid rafts" [recently renamed "membrane rafts" (*12*)], which are defined as small (10−200 nM) dynamic sterol- and sphingolipid-enriched structures. Membrane rafts are believed to compartmentalize cellular processes (*12*−*14*), and accordingly, association with membrane rafts might be important for the function of several membrane proteins (*13*−*16*). For the neurotransmitter transporters, evidence suggests that membrane raft association regulates targeting and function of glutamate transporters, especially EAAT2 (excitatory amino acid transporter 2) (*17*). Membrane raft association has also been suggested for the SERT in brain synaptosomes (*18*, *19*) and for NET in a trophoblast cell line in which the NET is endogenously expressed (*20*). Interestingly, the data suggested that the membrane raft association of NET may be critical for internalization of the transporter in response to protein kinase C activation (*20*).

The microenvironment and thus putative microdomain association of a given protein can be studied with a broad variety of technologies (*21*). These include techniques based on fluorescence that allow direct dynamic assessment of protein motions in living cells; i.e., microdomain association is defined by altered lateral diffusion properties in the membrane of the protein of interest. Two examples are FCS (fluorescence correlation spectroscopy) and FRAP (fluorescence recovery after photobleaching) (*21*). FCS employs a confocal microscope for visualizing the cells and a laser to define a very small volume (approximately 1 fL) which the fluorescent molecules traverse (*22*, *23*). Accordingly, FCS allows for real-time monitoring of fluorescently tagged proteins in living cells and even is sufficiently sensitive to detect single molecules (*22*, *23*). Interestingly, FCS has recently been used to assess the substrate binding stoichiometry and kinetics of the norepinephrine transporter with the help of a fluorescent substrate (*24*). FRAP is another and more established technique for examining the mobility of fluorescent proteins in living cells (*21*, *25*). It differs from FCS in the larger size of the sampling area and also the large number of fluorescent molecules analyzed (thousands rather than tens). In addition, FRAP experiments rely upon the destruction of fluorophores by bleaching to establish a background in which to examine fluorescence recovery in the bleached region (*21*).

In this study, we test the hypothesis that the DAT is associated with specific microdomains in the plasma membrane and that these operate to ensure proper spatial and temporal regulation of transporter function. We employ FCS and FRAP to assess the membrane mobility of the human DAT, tagged with yellow fluorescent protein (YFP-DAT) in non-neuronal cells and neuronally derived cells. By comparing the YFP-DAT with two other membrane proteins, EGFP-tagged EGFR (epidermal growth factor receptor) and β2AR (β2 adrenergic receptor), we obtain evidence for unique lateral diffusion profiles for each of the tested proteins in HEK293 cells and Neuro2A (N2a) cells. We also find that the unique diffusion properties of DAT likely are related to membrane raft and/or cytoskeleton association of the transport protein, and we provide evidence that the raft association might be critical for regulating transport capacity. The study is the first to jointly describe the membrane mobility of a biogenic amine neurotransmitter transporter and compare FCS- and FRAP-generated diffusion coefficients for membrane and cytoplasmic proteins. In addition, the data support the suggestion that the two techniques divulge more complementary than identical information about protein lateral diffusion.

EXPERIMENTAL PROCEDURES

DNA Constructs. The cDNA encoding YFP was fused to the N-terminus of a synthetic human DAT gene (kindly provided by J. Javitch, Columbia University, New York, NY) and cloned into the pCIHygro bicistronic mammalian expression vector (*26*, *27*). EGFP-DAT+Ala (EGFP fused to the N-terminus of the human DAT) was generated as described previously (*10*). FLAG-hDAT was generated by tagging the N-terminus of the synthetic human DAT gene with a FLAG epitope (Asp-Tyr-Lys-Asp-Asp-Asp-Asp-Lys). The construct was cloned into the pcDNA3 mammalian expression vector (Invitrogen). EGFP-PICK1 in the pEGFP N2 vector from Clontech was kindly supplied by K. Dev (Novartis, Zurich, Switzerland). EGFP-EGFR (epidermal growth factor receptor fused to EGFP) in pEGFP N1 (Clontech) and TfR-EGFP (EGFP fused to the C-terminus of the transferrin receptor) in pJPA5 were kindly provided by B. van Deurs, University of Copenhagen, Denmark.

Cell Culture and Transfection. HEK293 and mouse Neuro2a (N2a) neuroblastoma cells were maintained at 37 °C in 5% CO_2 in DMEM with Glutamax1 supplemented with 10% fetal bovine serum and 0.01 mg/mL gentamicin (all products from Invitrogen). For transient transfections, ~1 million cells were transfected with 2−4 μg of DNA/60 mm dish using either Lipofectamine in a 1:3 ratio (HEK293 cells) or Lipofectamine 2000 (both from Invitrogen) in a 1:4 ratio (N2a cells). The cells were plated onto 2× poly-D-lysine-coated Lab-Tek eight-well coverglass chamber slides (Nalge Nunc International, Naperville, IL) 24 h after transfection and analyzed 48−72 h post-transfection in phenol red free media as indicated. For stable expression, HEK293 cells were transfected with 5 μg of pCIHygro-YFP-DAT, and a stably transfected pool clone was selected using G418 (0.5 mg/mL) (Invitrogen). The cell lines were maintained in 0.2 mg/mL G418.

Confocal Fluorescence Microscopy and FCS. Confocal images were obtained and FCS measurements performed using an LSM 510 confocal microscope combined with the ConfoCor 2 system (Carl Zeiss, Jena, Germany). YFP-tagged proteins were excited at 514 nm with an argon laser through a 40× water-immersion objective (C-Apochromat), and the excitation was separated from the emission with a dichroic beam splitter. The resulting light was passed through a 530 nm long pass filter. For EGF-containing proteins, excitation was carried out at 488 nm and the emitted light measured through a 530 nm long pass filter. The tunable filter of the argon laser was used to create a low intensity to prevent photobleaching of the molecules. For purposes of FCS data collection, the pinhole in front of the avalanche photodiode was set to the manufacturer's suggested value of 74 μm to allow for optimized slice imaging with reduced out-of-plane

fluorescence. FCS measurements were conducted at the peak of fluorescence intensity, elucidated by performing a Z scan of 1 μm increments through the cell after it had been imaged. The fluorescence temporal signal was recorded, and the autocorrelation function $G(t)$, which yields the rate of fluctuation decay averaged over many fluctuations and reflects the particle number and the diffusion time (the half-time for correlation decay, τ_d), was calculated with the internal correlator. Curve fittings were carried out using ConfoCor, with a triplet state identified in the fitting, and two-dimensional fitting approximated by setting the structure parameter to 1000 (structure parameter = 5 for three-dimensional fitting). The beam waist of the 514 and 488 nm laser lines was calculated to be 0.18 and 0.19 μm, respectively, on the basis of the known diffusion coefficient of rhodamine in solution ($D = 28 \times 10^{-9}$ m^2/s). The diffusion coefficients of the labeled proteins were determined using the calibrated beam waist and the diffusion time obtained from the autocorrelation curve via the equation (*28*)

$$D = \omega_1^2/4\tau_D \quad (1)$$

where ω_1 is the beam waist and τ_D is the diffusion time. A minimum of three cells from at least three separate experiments were examined. The autocorrelation curve was generated from 10 × 10 s data collections. All experiments were carried out at 22 °C.

Fluorescence Recovery after Photobleaching. Cells were transfected and plated as described above. Appropriate cells for FRAP examination were visualized with the LSM 510 confocal microscope using the laser lines and filters described above. Spot photobleaching using circular regions of interest (ROIs) 1−3 μm in diameter were placed on the membrane or cytoplasm of the visualized cell, followed by illumination of the region with the appropriate laser line to obtain 30−70% bleaching compared to the prebleach image. The pinhole was kept fully open to ensure complete bleaching through the cell. The transmission intensity was no higher than 1%, and the bleaching of the sample due to imaging was negligible according to experiments with fixed cells (data not shown). Data were collected every 500 ms for an average of 1 min. Measurements up to 5 min were also performed, with no change in diffusion time or mobile fraction observable after the first minute. Images were processed with Photoshop 6.0 (Adobe, San Jose, CA), and recovery curves were calculated using nonlinear least-squares fits in ORIGIN 5.0 (OriginLab, Northampton, MA) set to the general equation for FRAP as described by Yguerabide et al. (*28*). The diffusion coefficient was determined using eq 1, where ω is the radius of the ROI set in the Zeiss program and the τ_D is determined from the fit of the recovery curve. Because the thickness of the cell was smaller than the bleached volume in the z direction, eq 1 was used to determine diffusion coefficients for cytoplasmic and membrane proteins. Three to six cells were examined in each experiment; experiments were performed a minimum of three times. Results are reported as the average ± the standard error. All measurements were carried out at 22 °C.

Preparation of Synaptosomes. The housing and care of the rats [male, Sprague-Dawley rats (Charles-River, Wilmington, MA), weighing 200−250 g] followed the guidelines of the Guide for the Care and Use of Laboratory Rats (Institute of Laboratory Animal Resources on Life Sciences, National Research Council, 1996). Rats were rapidly decapitated, and the brains were collected in ice-cooled dishes. The striatum was rapidly dissected and collected in 10 volumes (w/v) of 0.32 M cold sucrose. The tissue was immediately homogenized using a Teflon−glass homogenizer under chilled water and centrifuged at 1000*g* for 15 min at 4 °C. The resulting supernatant was centrifuged at 15000*g* for 20 min, and the pellet was washed by being resuspended in 0.32 M sucrose. The synaptosomes were suspended in regular KRH buffer saturated with 95% O_2 and 5% CO_2. Protein concentrations were determined by DC protein assay (Bio-Rad) using bovine serum albumin as a standard. The purified synaptosomal preparation was used immediately for experiments. The striatum was pooled from four rats for an experiment, and all the experiments were repeated at least three times.

Membrane Raft Isolation by Sucrose Gradient Centrifugation. Sucrose gradient centrifugation was used to separate membrane rafts as described previously (*19*, *20*). For experiments performed on cells, transiently transfected N2a cells expressing FLAG-hDAT were lysed in MBS buffer [25 mM MES and 150 mM NaCl (pH 6.5) containing 0.4% Triton X-100 and protease inhibitors 1 μM pepstatin A, 250 μM PMSF, 1 mg/mL leupeptin, and 1 μg/mL aprotonin]. The extraction procedure ensured a detergent:protein ratio of 10−15. Equal volumes of 80% (w/v) sucrose were added to the homogenate. All sucrose solutions contained the same buffer composition, detergent, and protease inhibitors. Lysed samples (3.8 mL) in 40% sucrose were overlaid successively with 3.8 mL of 30% sucrose and 3 mL of 5% sucrose in a Beckman SW41 ultracentrifuge tube. Following centrifugation at 188000*g* for 18 h at 4 °C, 0.9 mL fractions were collected from the top. Total proteins in each fraction were precipitated with 10% cold trichloroacetic acid, washed in acetone, air-dried, and subjected to 4 to 15% linear gradient SDS−PAGE. The proteins were transferred to PVDF membrane, and the presence of DAT and other proteins was assessed by immunoblotting with specific antibodies (*20*). For detection of GM1, 10 μL of each fraction was applied to a nitrocellulose membrane using dot-blot apparatus (Bio-Rad) and probed with 10 ng/mL horseradish peroxidase-coupled cholera toxin β-subunit (CTB).

For experiments on synaptosomes, the striatal synaptosomes (prepared as described above) were suspended at a density of 5 mg of protein/mL of MBS buffer [25 mM MES and 150 mM NaCl (pH 6.5) containing 0.4% Triton X-100 and protease inhibitors 1 μM pepstatin A, 250 μM PMSF, 1 mg/mL leupeptin, and 1 μg/mL aprotonin] (*29*). Synaptosomes were lysed using a Dounce homogenizer with 10 up and down strokes at 4 °C and then passed through a 27.1/2 gauge needle. Equal volumes of 80% (w/v) sucrose were added to the homogenate. All sucrose solutions contained the same buffer composition, detergent, and protease inhibitors. Lysed samples (4 mL) in 40% sucrose were overlaid successively with 4 mL of 30% sucrose and 3 mL of 5% sucrose in a Beckman SW41 ultracentrifuge tube. Following centrifugation at 188000*g* for 18 h at 4 °C, 1 mL fractions were collected from the top. The pellet was resuspended in 1 mL of detergent buffer by brief sonication. Total proteins in each fraction were precipitated as described for the

experiments on cells with 10% cold trichloroacetic acid, washed in acetone, air-dried, and subjected to 4 to 15% linear gradient SDS−PAGE. Immunoblotting and CTB dot blots were performed as described above for the experiments with cells.

Uptake Experiments. Uptake assays in cells were performed using [2,5,6-^{3}H]dopamine (7−21 Ci/mmol) (Amersham, Little Chalfont, U.K.). The [^{3}H]dopamine uptake assay was performed on whole cells 3 days after transfection. The day after transfection, the cells were seeded at a density of 0.5×10^5 cells/well in 24-well plates coated with 20 mg/mL poly-D-lysine (Sigma) in PBS (phosphate-buffered saline) buffer. After the plates had been seeded, they were left for 2 days in the incubator. Prior to the experiment, the cells were washed once in 250 μL of uptake buffer [25 mM HEPES (pH 7.4) with 130 mM NaCl, 5.4 mM KCl, 1.2 mM $CaCl_2$, 1.2 mM $MgSO_4$, 1 mM L-ascorbic acid, 5 mM D-glucose, and 1 μM catechol *O*-methyltransferase inhibitor Ro 41-0960 (Sigma)]. Next, 200 μL of uptake buffer and 25 μL of unlabeled dopamine (RBI, Natick, MA) were added (final assay concentrations of dopamine ranged from 10 nM to 1 mM). Uptake was initiated by addition of ~90 nM [^{3}H]dopamine in 25 μL of uptake buffer. After incubation for 3 min at 37 °C, the cells were washed twice with 250 μL of ice-cold uptake buffer, lysed in 250 μL of 1% sodium dodecyl sulfate (SDS), and left for 1 h at 37 °C. All samples were subsequently transferred to 24-well counting plates (Perkin-Elmer Life Sciences, Boston, MA) followed by addition of 400 μL of Opti-phase HiSafe 3 scintillation fluid (Perkin-Elmer Life Sciences). The samples were counted in a Wallac Tri-Lux β scintillation counter (Perkin-Elmer Life Sciences). All determinations were performed in triplicate.

Uptake experiments on synaptosomes with DA were performed essentially as described previously (*19*). Briefly, 25−50 μg of purified synaptosomes was incubated in 250 μL of Krebs-Ringer-HEPES (KRH) buffer (120 mM NaCl, 4.7 mM KCl, 2.2 mM $CaCl_2$, 10 mM HEPES, 1.2 mM $MgSO_4$, 1.2 mM KH_2PO_4, 5 mM Tris, and 10 mM D-glucose) containing 0.1 mM ascorbic acid, 0.1 mM pargyline, and 40 nM [^{3}H]DA for at pH 7.4 3 min. Synaptosomes were preincubated with the mβCD (3.75 mM) and or DAT inhibitor at 37 °C for 10 min followed by the addition of [^{3}H]DA. Nonspecific [^{3}H]DA uptake was defined as the accumulation in the presence of 0.1 μM nomifensine and was subtracted from total uptake. Uptake was terminated with the addition of 3 mL of ice-cold PBS followed by rapid filtration over 0.3% polyethylenimine-coated GF-B filters on a Brandel cell harvester. Filters were washed rapidly with 5 mL of cold PBS, and radioactivity bound to the filter was counted with a liquid scintillation counter. Mean values of specific uptake ± the standard error of at least three separate experiments were determined.

Cholera Toxin Patching. N2a cells transiently tranfected with either pCIHygro EGFP-DAT or pJPA5 TfR-EGFP were seeded on glass cover slides treated with polyornithine in six-well plates (250 000 cells/well). The cells were used for experiments 3 days after transfection. Cholera toxin patching was performed essentially as described by Chmelar and Nathanson (*30*). In brief, cells were incubated on ice for 30 min with Alexa-647-conjugated cholera toxin β-subunit (CTB, 10 μg/mL) (Molecular Probes) in DMEM-HEPES containing 0.2% BSA. After the incubation, the cells were rinsed three times in ice-cold PBS. For the unpatched condition, cells were fixed in 4% paraformaldehyde in PBS and rinsed three times in PBS. The specimens were subsequently mounted in AntiFade (Molecular Probes) on glass slides. Patching of CTB was achieved by incubating the cells with rabbit anti-CTB (1:100 in DMEM-HEPES and 0.2% BSA; Sigma) for 20 min at 37 °C. The cells were then removed from the incubator, rinsed three times in ice-cold PBS, fixed in 4% paraformaldehyde for 20 min on ice, and mounted with SlowFade (Molecular Probes) on glass slides. Specimens were examined using a Zeiss LSM510 confocal laser microscope with an oil immersion 63×/1.4NA objective, using instrument settings avoiding cross talk between channels, and pixel saturation. Images were obtained through the center of the cell with an estimated section thickness of 0.7 μm. Quantification of colocalization was achieved using the RG2B colocalization plug-in to ImageJ (W. S. Rasband, National Institutes of Health, Bethesda, MD, 1997−2006) as described by Chmelar and Nathanson (*30*). The plasma membrane area of cells expressing the EGFP-tagged DAT or TfR was defined as the region of interest to avoid noise from untransfected cells and nonspecific staining. A minimum threshold pixel intensity of 50 was set for each channel to reduce background noise, and the minimum ratio for pixel intensity between the two channels was set to 0.5. Results are displayed as percent colocalization as determined by dividing the area of colocalization pixels by the total area over the threshold of the limiting channel (Alexa-647 CTB). Fifteen or sixteen cells were used for quantification under each condition. Statistical significance was determined using a Student's *t*-test. Differences were considered significant when $p < 0.05$.

Surface Biotinylation. Transiently transfected N2a cells were seeded in six-well plates at a density of 400 000 cells/well. After 2 days, the cells were treated with DMEM with or without mBCD for 30 min at 37 °C. The cells were washed in ice-cold PBS (phosphate-buffered saline) and labeled with Sulfo-NHS-SS-Biotin (Pierce Research Chemicals Inc.) for 40 min on ice. The remaining Sulfo-NHS-SS-Biotin was removed and quenched with two washes in TBS (Tris-buffered saline). Cells were solubilized in TBS containing 1% Triton X-100, 0.1% SDS, and a protease inhibitor mixture tablet (Roche Diagnostics). After the mixture was rotated 10 min, insoluble debris was removed by centrifugation (20000*g* for 30 min at 4 °C). Resulting supernatants (500 μg of protein) were incubated with monomeric avidin beads (175 μL) (Pierce) for 1 h at room temperature. The beads were washed four times with solubilization buffer before elution with 50 μL of 2× loading buffer [100 mM Tris-HCl (pH 6.8), 20% glycerol, 10% SDS, 0.1 M DTT, and 0.2% bromophenol blue] for 30 min at room temperature. The eluates were analyzed by 10% SDS−PAGE, transferred to a nitrocellulose membrane, and blotted with MAB369 anti-DAT antibody (Chemicon) and secondary horseradish peroxidase-coupled goat anti-mouse antibody (Pierce) in blocking solution (TBS buffer with 5% Carnation dry milk and 0.05% Tween 20). The protein was visualized with ECL+ according to the manufacturer's protocol (Amersham Biosciences).

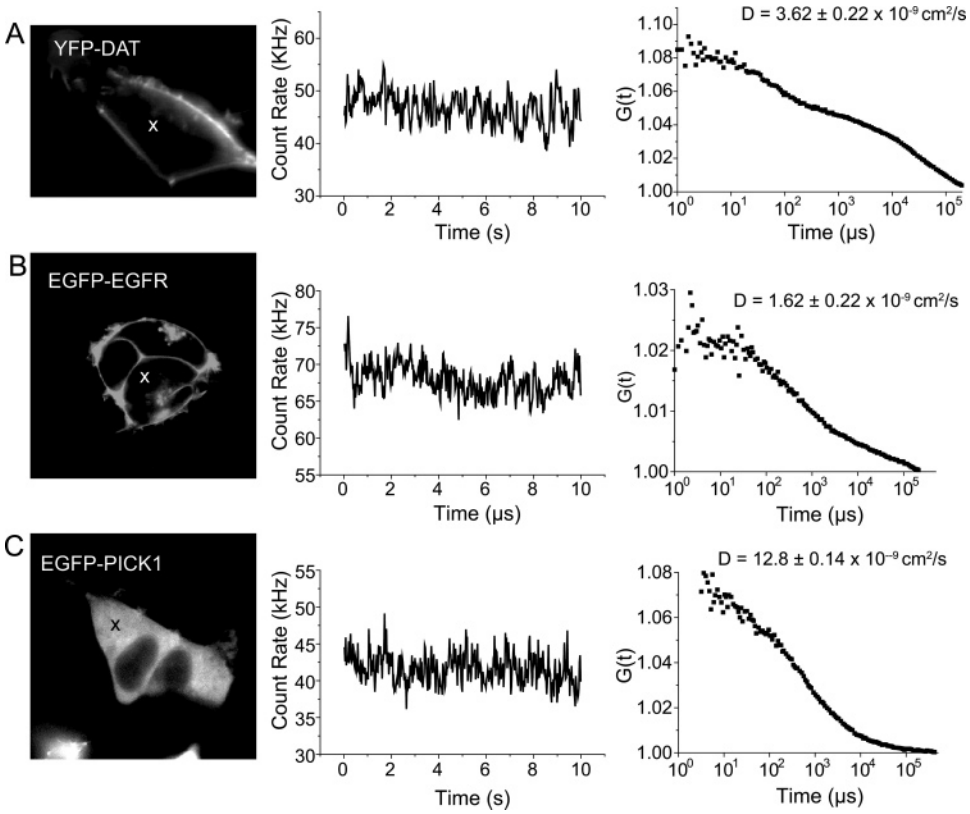

FIGURE 1: FCS analysis in HEK293 cells expressing YFP-DAT, EGFP-EGFR, or EGFP-PICK1. The indicated constructs [(A) YFP-DAT, (B) EGFP-EGFR, and (C) EGFP-PICK1] were stably expressed in HEK293 cells, and FCS measurements were taken at 22 °C as described in Experimental Procedures. Confocal images (left panels) were captured using an argon laser with a 488 nm line for EGFP and a 514 nm line for YFP. The middle panels depict representative 10 s measures (out of 10) of the fluorescence intensity fluctuations from which the autocorrelation functions $G(t)$ were calculated. The fluctuations are reflective of the fluorescence signal from the fluorescent molecules traveling through the confocal volume. The right panels show autocorrelation functions calculated with the internal correlator from the fluorescence intensity fluctuations shown in the middle panels. The diffusion times (τ_D) corresponding to the half-times for the correlation decay were determined from each of the autocorrelation functions and the indicated diffusion coefficients D (means ± standard error of at least three independent experiments) calculated via the equation $D = \omega_1^2/4\tau_D$, where ω is the beam waist and τ_D is the diffusion time (*29*). An X has been placed on the cell image indicating where the FCS measurement was taken. The X corresponds to the membrane region above the nucleus for YFP-DAT and EGFP-EGFR and corresponds to the cytosol for EGFP-PICK1.

RESULTS

FCS was performed using the commercially available ConfoCor2/LSM 510 system from Zeiss, which allows for both imaging of the fluorescent protein and examination of its dynamic properties. To evaluate the amenability of FCS to our transporter, we established a pool clone of HEK293 cells stably expressing the hDAT tagged at the N-terminus with YFP (YFP-DAT). This tag did not significantly alter the functional properties of the transporter as assessed in [^{3}H]-dopamine uptake experiments (data not shown) and in agreement with previous data (*31*). Representative results shown in Figure 1 show that YFP-DAT was almost exclusively expressed at the plasma membrane with little or no intracellular staining. FCS readings from these cells provided a proper fluctuating fluorescent signal derived from the fluorescent molecules traveling through the confocal space (Figure 1A). The count rate was stable as reflected by a low threshold of background noise (experimentally determined as 2−5 kHz) and a lack of bleaching over the measuring time (Figure 1A). On the basis of the readings, the fluorescence fluctuation autocorrelation function was calculated. The calculated function $G(\tau)$, which yields the rate of fluctuation decay averaged over many fluctuations, was biphasic with a shorter diffusion time of approximately 100 μs representing the photophysical properties of the fluorophore (*32*, *33*) and a longer diffusion time (the half-time for correlation decay, τ_D) of approximately 20 ms for the fluorescent DAT (Figure 1A). From the diffusion time τ_D, we calculated the diffusion coefficient D using eq 1 (see Experimental Procedures) to be $(3.62 \pm 0.22) \times 10^{-9}$ cm^2/s, which suggests a relatively freely diffusible membrane protein in the HEK293 cells (*34*). Note that similar diffusional properties were observed for YFP-DAT transiently transfected into HEK293 cells (data not shown). For comparison, we expressed EGFR tagged with EGFP in HEK293 cells. EGFP-EGFR displayed a somewhat slower diffusion than YFP-DAT [$D = (1.62 \pm 0.22) \times 10^{-9}$ cm^2/s vs $(3.62 \pm 0.22) \times 10^{-9}$ cm^2/s (Figure 1B)]; however, the value was directly comparable to previously reported values for this receptor in Chinese hamster ovary cells using FCS [$(1.6 \pm 0.9) \times 10^{-9}$ cm^2/s] (*35*). For additional comparison, we analyzed a cytosolic protein. We chose PICK1, an interaction partner of the DAT (*9*, *10*). Transfection of PICK1, tagged at the N-terminus with EGFP, into HEK293 cells resulted in a uniform distribution of the protein within the cytosol (Figure 1C). As expected, FCS revealed a significantly faster diffusion coefficient [$(12.8 \pm 1.4) \times 10^{-9}$ cm^2/s (Figure 1C)] for EGFP-PICK1 compared to those obtained for YFP-DAT and EGFP-EGFR (Figure 1A,B).

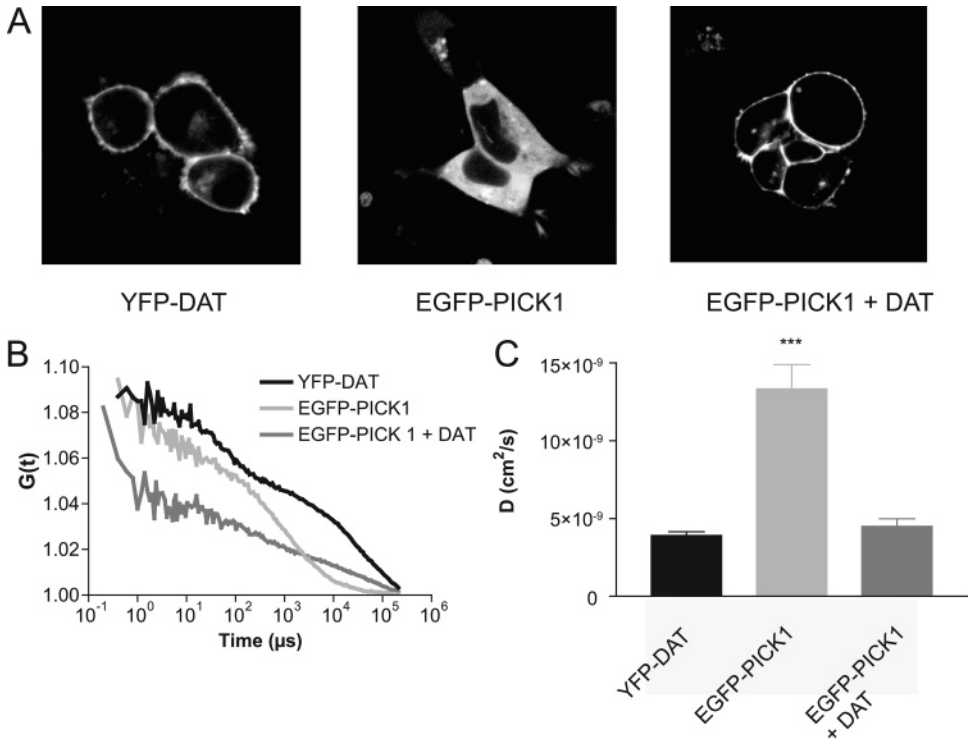

FIGURE 2: FCS analysis of EGFP-PICK1 alone and upon coexpression with DAT. (A) Confocal images of HEK293 cells expressing YFP-DAT, EGFP-PICK1, and the DAT with EGFP-PICK1. The images were captured using an argon laser with a 488 nm line for EGFP and a 514 nm line for YFP. (B) Autocorrelation curves for the indicated constructs. The autocorrelation functions $G(t)$ were calculated from the raw fluorescence fluctuation data with the internal correlator. (C) Calculated diffusion coefficients (D) (means ± standard error; $n = 10$). The diffusion times (τ_D) corresponding to the half-times for the correlation decays were determined from each of the autocorrelation functions and the indicated diffusion coefficients D calculated via the equation $D = \omega_1^2/4\tau_D$, where ω is the beam waist and τ_D is the diffusion time (*29*).

We also stably expressed EGFP-PICK1 together with the DAT and compared those cells with cells stably expressing only EGFP-PICK1. Coexpression with the DAT resulted in recruitment of PICK1 to the plasma membrane (Figure 2A). Examination of the diffusion coefficient of EGFP-PICK1 with the DAT showed that the fluorescent protein acquired a much slower diffusion, similar to that observed for YFP-DAT (Figure 2B). The data support the possibility of using FCS and thus diffusion properties to assess a cellular protein−protein interaction.

Next we compared the lateral mobility of the DAT in HEK293 with that in neuronally derived Neuro2A (N2a) cells. In these cells, YFP-DAT was expressed at high levels at the plasma membrane and was fully functional (data not shown). We were, however, unable to perform a reliable FCS analysis in the N2a cells transiently expressing YFP-DAT due to massive bleaching of fluorescent molecules. This bleaching phenomenon observed in the count rate is manifested as a flat autocorrelation curve and most likely indicates a relative immobilization of YFP-DAT in N2a cells (Figure 3). Note that similar bleaching behaviors have been seen in other FCS studies in mammalian cells (*36*). Our inability to perform FCS on YFP-DAT in N2a cells was not a general phenomenon. By analyzing N2a cells transiently expressing EGFP-PICK1, we were able to capture reliable FCS data with a stable count rate (i.e., the photon counts per molecule per second) and a calculated diffusion coefficient of $\sim 11 \times 10^{-9}$ cm^2/s (data not shown), which corresponded well with the value obtained for PICK1 expressed in HEK293 cells (Figure 1C).

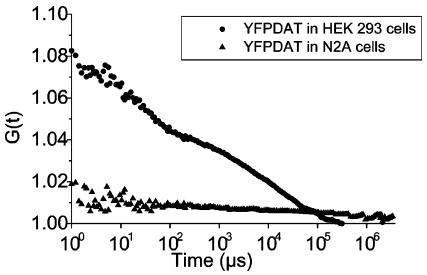

FIGURE 3: Photobleaching of YFP-DAT in N2a cells but not in HEK293 cells. Two representative autocorrelation curves were obtained from YFP-DAT in HEK293 cells (●) and N2a cells (▲). The autocorrelation functions $G(t)$ were calculated from the raw fluorescence fluctuation data with the internal correlator. The lack of correlation for YFP-DAT in N2a cells as reflected in the flat autocorrelation curve is likely due to a constant bleaching of fluorescent molecules in the confocal volume, consistent with an immobile or slowly moving population of fluorescent molecules.

The inability to measure a diffusion time for YFP-DAT expressed in N2a cells using FCS led us to another technique for assessing protein dynamics, FRAP. We assayed the diffusion of YFP-DAT in N2a cells using a circular bleach spot with an average diameter of 3 μm. The bleaching was performed at the edge of the membrane, and a representative bleaching and recovery of YFP-DAT in N2a and HEK293 cells is shown in panels A and B of Figure 4. The white arrow indicates the bleached region and its subsequent recovery. The collected images and the resulting recovery curve showed, as would be predicted from our inability to use FCS, an overall slower diffusion in N2a cells compared to HEK293 cells with diffusion coefficients (D) of (0.127

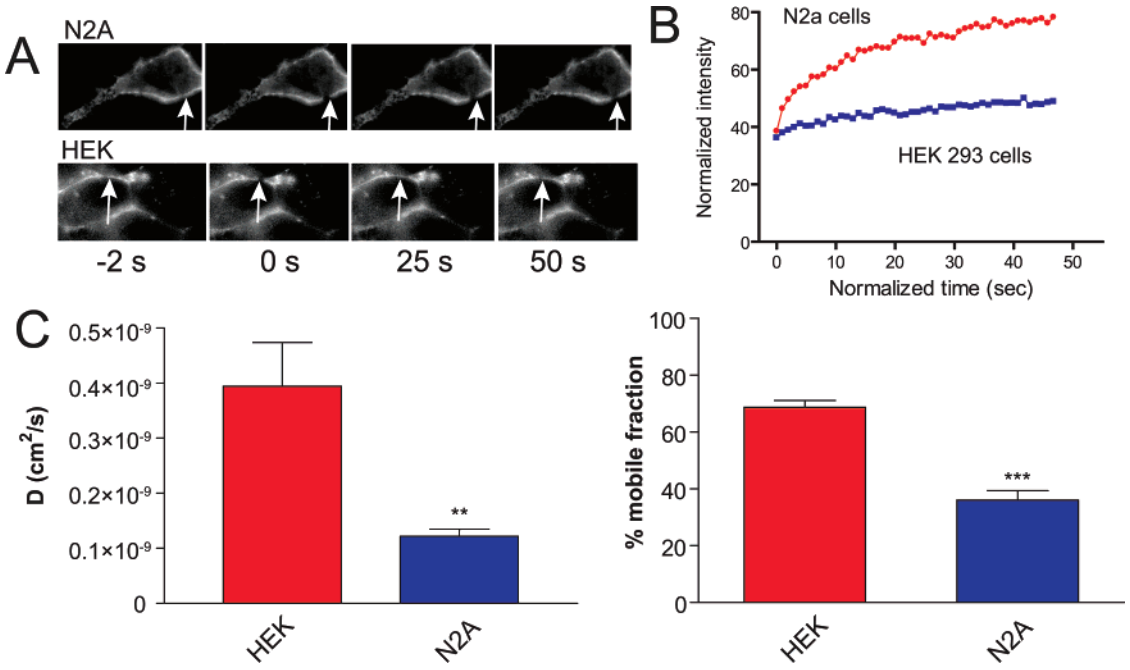

FIGURE 4: Lateral mobility of YFP-DAT in HEK293 cells and N2a cells assessed by FRAP. (A) Visual comparison of YFP-DAT fluorescence at indicated time points after photobleaching in N2a and HEK293 cells. The bleached spot is indicated by the arrows. (B) Fluorescence recovery curves for YFP-DAT in N2a and HEK293 cells. Bleaching was done to approximately 35% of the initial fluorescence, upon which recovery was measured as indicated by the curves. The data are shown as the normalized fluorescence intensity as a function of time (seconds). (C) Diffusion coefficients and mobile fractions calculated on the basis of FRAP experiments in N2a and HEK293 cells. The FRAP measurements and calculations were performed as described in Experimental Procedures. Data are means ± standard error ($n = 10$). Two asterisks indicate a p of <0.01 and three asterisks a p of <0.001 (t-test).

± 0.012) × 10^{-9} and (0.307 ± 0.035) × 10^{-9} cm^2/s, respectively ($p < 0.01$, t-test). Furthermore, the mobile fraction of YFP-DAT, defined as the maximum fractional recovery estimated from the recovery curves, was markedly smaller in N2a cells (36 ± 3%) than in HEK293 cells (69 ± 2%, $p < 0.0001$, t-test) (Figure 4D). To control for the possibility of bleaching during image acquisition in FRAP, cells expressing YFP-DAT were fixed and a bleaching profile was gathered. After the initial bleaching of an area to approximately 50% of its original fluorescence, we monitored any bleaching due to scanning the image; however, the observed bleaching was negligible (data not shown). Note that the diffusion coefficient (D) for YFP-DAT in HEK293 cells obtained with FRAP is almost one order of magnitude smaller than that obtained with FCS. As discussed later, we believe that this apparent discrepancy reflects some inherent differences in what the two techniques measure.

To assess whether other membrane proteins have a differential diffusion and mobile fraction in N2a as compared to HEK293 cells, we performed FRAP analysis for EGFP-EGFR (epidermal growth factor receptor) and EGFP-β2AR (β2-adrenergic receptor). In HEK293 cells, the diffusion coefficients for EGFP-EGFR exhibited little difference from that of YFP-DAT, but EGFP-β2AR was significantly slower than YFP-DAT (Figure 5A). However, the mobile fraction of EGFP-β2AR was not different from YFP-DAT, whereas the mobile fraction for EGFP-EGFR was significantly greater (Figure 5B). A different picture emerged in N2a cells, with EGFP-EGFR and EGFP-β2AR both displaying significantly faster diffusion coefficients compared to that of YFP-DAT (Figure 5C). Correspondingly, the smaller mobile fraction observed for YFP-DAT was not observed for EGFP-β2AR or EGFP-EGFR (Figure 5D). The results support the notion that distinct membrane proteins associate with different ensembles of cellular proteins and lipid environments that in turn might result in distinct mobility in the plasma membrane.

To explore the molecular basis for the relative immobilization of YFP-DAT in N2a cells, we first tested the hypothesis that interaction with PDZ domain-containing scaffolding proteins was critical for microdomain association of YFP-DAT in N2a cells. This hypothesis was fueled by the finding that PICK1, a PDZ domain-containing scaffolding protein that binds the DAT C-terminus (*9*, *10*), is strongly expressed in N2a cells (J. Fog and U. Gether, unpublished observation). Accordingly, we expressed in N2a cells a mutant DAT with an extra alanine added to the C-terminus, a mutation known to disrupt the interaction between the DAT and the PDZ domain proteins of PICK1 (*10*). In contrast to our expectations, the mutant (EGFP-DAT+Ala) exhibited a similarly slow diffusion coefficient like that of YFP-DAT, and in addition, the mobile fraction was unchanged (Figure 5).

Next, we wanted to test the hypothesis that the low lateral mobility of YFP-DAT in N2a cells was the result of association of the DAT with membrane rafts and/or the cytoskeleton. We applied raft-disrupting and cytoskeleton-disrupting reagents and examined their effect on the lateral diffusion of the DAT in the plasma membrane. Application of the cholesterol-extracting reagent mβCD (*13*) caused a significantly faster lateral diffusion of YFP-DAT in the plasma membrane (Figure 6A). Similarly, we observed that the cytoskeleton-disrupting agent cytochalasin D (2 μM) significantly enhanced the diffusion coefficient for YFP-DAT. In contrast, lateral diffusion did not change for EGFP-EGFR in response to either mβCD or cytochalasin D (Figure 6B). With regard to the mobile fractions we observed for

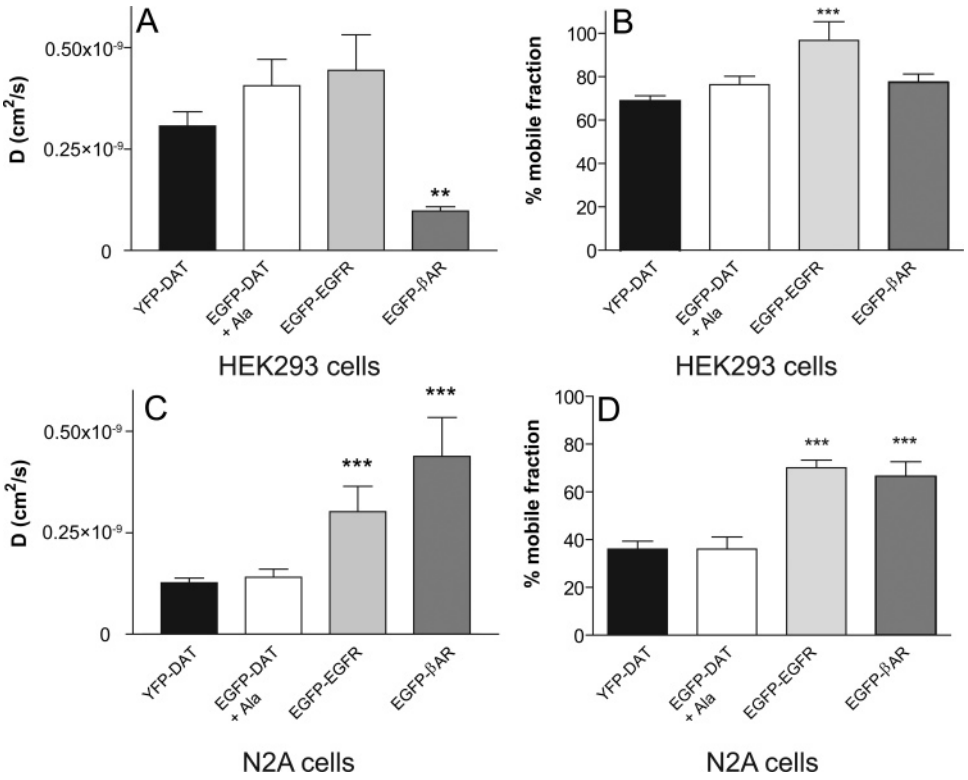

FIGURE 5: FRAP analysis of YFP-DAT in comparison to EGFP-DAT+Ala, EGFP-EGFR, EGFP-β2AR, and EGFP-PICK1 in HEK293 and N2a cells. (A and B) Diffusion coefficients and mobile fraction recovery for YFP-DAT, EGFP-DAT+Ala, EGFP-EGFR, EGFP-β2AR, and EGFP-PICK1 in HEK293 cells. (C and D) Diffusion coefficients and mobile fraction recovery for YFP-DAT, EGFP-DAT+Ala, EGFP-EGFR, EGFP-β2AR, and EGFP-PICK1 in N2a cells. Data are means $\pm$ the standard error of at least five independent experiments. Two asterisks indicate a p of <0.0025 and three asterisks a p of <0.001; significance in each case is in comparison to YFP-DAT (one-way ANOVA with Bonferroni's multiple-comparison test).

YFP-DAT, minor though statistically insignificant increases in the mobile fractions (53 $\pm$ 4% for mβCD and 47 $\pm$ 6.0 for cytochalasin D vs 43 $\pm$ 3% for control, means $\pm$ standard error; $n = 7-12$). For EGFP-EGFR, the mobile fractions were 70 $\pm$ 3% for EGFP-EGFR and vehicle, 75 $\pm$ 2% for EGFP-EGFR and mβCD, and 77 $\pm$ 12 for EGFP-EGFR and cytochalasin D (means $\pm$ standard error; $n = 3$). Taken together, the results indicate that raft association of the DAT and/or cytoskeleton association is important for the unique lateral diffusion properties of YFP-DAT in N2a cells.

To address biochemically whether DAT was associated with membrane rafts, we prepared extracts with 0.4% Triton X-100 from N2a cells transiently expressing the DAT and performed sucrose density gradients. The proteins from the different fractions were separated by SDS−PAGE followed by immunoblotting. As illustrated in Figure 7, a significant fraction of the DAT protein was found in the membrane raft fractions. The membrane raft fractions were confirmed by the presence of membrane raft markers caveolin (not shown) and GM1 glycosphingolipids (Figure 7), and non-membrane raft fractions were confirmed by the presence of Na^+/K^+-ATPase (Figure 7) and the transferrin receptor (not shown). The localization of GM1 was detected by dot blotting with horseradish peroxidase-conjugated cholera toxin B-subunit (CTB) (Figure 7).

To further assess putative localization of the DAT to membrane rafts, we employed a CTB patching protocol (*30*, *37*, *38*). CTB pentavalently binds GM1 sphingolipids, resulting in coclustering of raft-associated proteins. This clustering can be further enhanced by cross-linking of CTB with anti-CTB antibodies, bringing complete lipid microdomains together in distinct microscopically visible patches within the membrane (*30*, *37*, *38*). The experiments were performed in N2a cells transiently expressing either EGFP-DAT or TfR-EGFP (transferrin receptor tagged with EGFP). Given that the TfR is usually not associated with membrane rafts (*37*), we chose this molecule as a negative control for our experiments. In the transfected N2a cells, EGFP-DAT was evenly distributed in the plasma membrane (Figure 8A). Similarly, staining of the cells with Alexa-647-conjugated CTB (Alexa647-CTB) resulted in a uniform staining of the plasma membrane, and an overlay of the images indicated quite extensive colocalization (Figure 8A). Patching of the bound Alexa647-CTB with anti-CTB antibody resulted in a markedly more punctuate staining (Figure 8B). It also resulted in a more punctuate localization of EGFP-DAT that corresponded well to that seen for Alexa647-CTB (Figure 8C). The overlap was not complete ($\sim$48% colocalization) as would be expected on the basis of the sucrose gradient data indicating only partial raft association of the DAT (Figure 7). Our control protein, TfR-EGFP, was also found in the plasma membrane but exhibited a more punctuate expression pattern also in nonpatched cells. Note that TfR-EGFP as expected also was found intracellularly where it likely was associated with recycling endosomes (Figure 8). As a consequence of the more punctuate expression of TfR-EGFP in the plasma membrane, an overlay with the Alexa647-CTB image indicated less apparent colocalization of the two proteins as compared to that seen for EGFP-DAT and Alexa647-CTB (Figure 8). Patching did also not alter

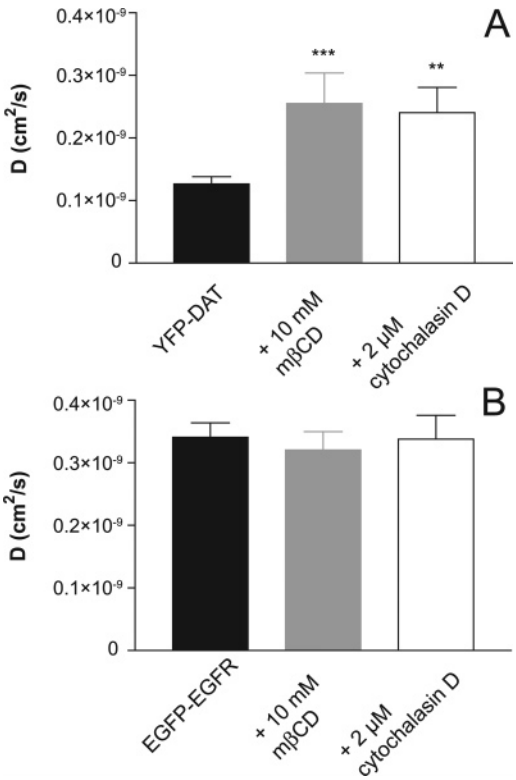

FIGURE 6: Effect of cholesterol depletion and cytoskeleton disruption on the lateral mobility of YFP-DAT and EGFP-EGFR in N2a cells. (A) Diffusion coefficients obtained by FRAP for YFP-DAT in N2a cells without and with incubation with 10 mM methyl-β-cyclodextrin (mβCD) or 2 μM cytochalasin D. (B) Diffusion coefficients obtained by FRAP for EGFP-EGFR in N2a cells without and with incubation with 10 mM mβCD or 2 μM cytochalasin D. Data are means $\pm$ the standard error ($n = 3$). Two asterisks indicate a p of <0.0025 and three asterisks a p of <0.001 (one-way ANOVA with a Kruskal−Wallis post hoc test).

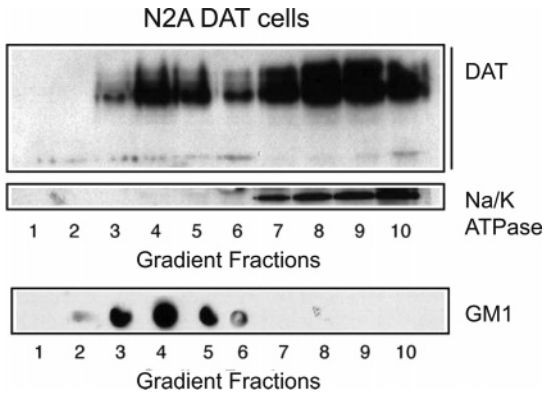

FIGURE 7: Presence of DAT in membrane raft and non-membrane raft fractions from N2a cells expressing DAT. N2a cells transiently expressing DAT were extracted with 0.4% Triton X-100, and sucrose density gradients were performed as described in Experimental Procedures. The proteins from fractions 1−10 (from top to bottom) were separated by SDS−PAGE and probed with antibodies against the indicated proteins. DAT proteins are found both in membrane raft fractions (3−5) and in non-membrane raft fractions (7−10). Membrane raft fractions were confirmed by the presence of the membrane raft marker GM1, and non-membrane raft fractions were confirmed by the presence of the Na^+/K^+-ATPase. The localization of the membrane raft marker ganglioside (GM1) was detected by dot blotting with horseradish peroxidase-conjugated cholera toxin B-subunit (CTXB) as described in Experimental Procedures. Representative immunoblots of five independent experiments are shown.

the punctuate expression pattern at the plasma membrane of TfR-EGFP. Moreover, the punctuate pattern observed for patched Alexa647-CTB colocalized markedly less with TfR-EGFP than the DAT (Figure 8C). The calculated colocalization of Alexa647-CTB with TfR-EGFP was ~30%, which is comparable to what others have calculated for non-raft-associated proteins using a similar quantification method (*30*, *37*, *38*). Taken together, the data provide additional support for partial localization of the DAT to membrane rafts.

To investigate whether membrane raft association of the DAT plays a role in transport function, we investigated the effect of mβCD on [^{3}H]dopamine uptake. The treatment caused a marked reduction both in the V_{max} value for uptake (Figure 9) and in the K_M value [control, $K_M = 0.57 \pm 0.11$ μM; mβCD, $K_M = 0.18 \pm 0.04$ μM (means $\pm$ standard error; $n = 3$, $p < 0.05$)]. Note that both in the presence and in the absence of mβCD the uptake curves displayed a Hill coefficient close to unity (Figure 9A). The alteration in the uptake parameters was not associated with a change in the amount of surface-expressed DAT as assessed by surface biotinylation experiments (Figure 9B,C). Thus, although an indirect effect of mβCD cannot be ruled out, the data suggest that raft association and/or cholesterol is critical for optimal DAT function. Unfortunately, we were unable to obtain reliable uptake when we treated the cells with cytochalasin D; i.e., the treated cells did not adhere sufficiently to the surface of the wells to withstand the repetitive washes required in our uptake assay.

The experiments described above were performed on transfected cells. We decided, therefore, also to test membrane raft association and the functional effects of cholesterol depletion on striatal synaptosomes containing endogenously expressed DAT. In agreement with our data obtained in N2a cells, sucrose density gradient experiments with rat striatal synaptosomes showed clear association of the DAT with the membrane raft fractions as determined by colocalizattion with GM1 glycosphingolipids (Figure 10A). In further agreement with our data in N2a cells, treatment with mβCD caused a marked reduction in the rate of [^{3}H]dopamine uptake in the striatal synaptosomes (Figure 10B).

Table 1 shows the comparison of diffusion coefficients generated by FCS and FRAP in HEK293 cells for YFP-DAT, EGFP-PICK1, and EGFP-PICK1 with the DAT. From these, it appears that whereas the D values for the cytoplasmic protein EGFP-PICK1 were similar for both FCS and FRAP, those for the membrane-localized proteins exhibited an order of magnitude difference between the two techniques. Because the differences lie only in measurements for membrane proteins, we speculated that this incongruity stems from the differential measuring of dissimilar microenvironments in the plasma membrane by the two methods. If this were the case, we would expect that reagents that can alter the physical properties of the plasma membrane might have a different impact on the measured lateral diffusion. In agreement with this prediction, we found that HEK293 cells treated with filipin (5 μg/mL, 1 h, 37 °C), which is known to cause cross-linking of cholesterol in the membrane, caused a deceleration of diffusion according to FRAP while diffusion was enhanced according to FCS (Figure 11A,B). Treatments with mβCD (10 mM, 30 min, 37 °C) recapitulated this effect, although to a lesser degree (data not shown), and cytochalasin D

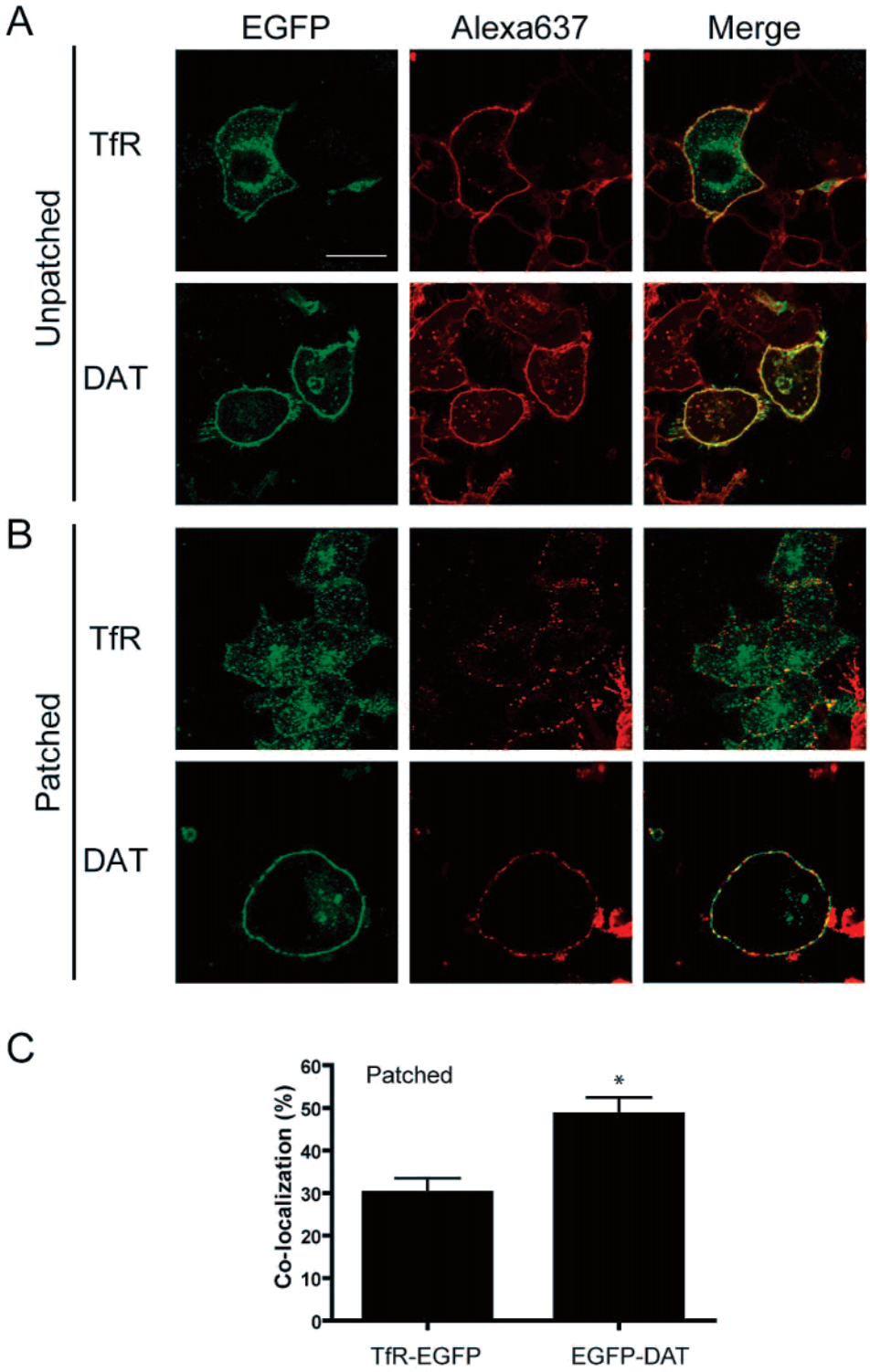

FIGURE 8: EGFP-DAT colocalizes with patched CTB. (A) N2a cells expressing either EGFP-DAT or TfR-EGFP were labeled with Alexa647-CTB and analyzed by confocal microscopy as described in Experimental Procedures. The left column shows the fluorescence from EGFP-tagged protein, the middle column the fluorescence from Alexa647-CTB, and the right column a merging of the two other images. (B) Labeling as in panel A with a subsequent patching with anti-CTB antibody. The scale bar is 20 μm. (C) Quantification of the colocalization between patched CTB and TfR-EGFP ($n = 15$ cells) or EGFP-DAT ($n = 16$ cells) as represented by the images in panel B. Data are means $\pm$ the standard error. The asterisk indicates a p of <0.05 compared to the value for TfR-EGFP (t-test).

(2 μM, 10 min, 37 °C) did not significantly alter the diffusion coefficients for either FCS or FRAP in the HEK293 cells (data not shown).

DISCUSSION

To assess microdomain association of the DAT and the putative functional implications, we have in this study employed a series of biophysical, biochemical, and pharmacological techniques in two different cellular systems. Our work included the use of FCS and FRAP to test the lateral mobility of the DAT in the plasma membrane (*22*, *23*). FCS is very gentle to the tissue sample as the fluorescence intensity that is employed is very low. Moreover, because the technique utilizes a very small volume, data are obtained

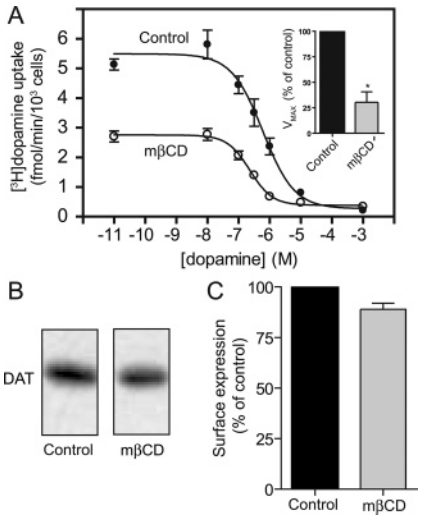

FIGURE 9: Effect of cholesterol depletion on the functional activity and surface expression of hDAT in N2a cells. (A) Effect of 10 mM mβCD on [^{3}H]dopamine uptake in N2a cells transiently expressing hDAT. Data are given as counts per minute (CPM) in the absence or presence of mβCD at the indicated concentrations of dopamine (means ± standard error of triplicate determinations). The experiment that is shown is representative of three identical experiments with similar results. The curves were derived from nonlinear regression analysis of the uptake data. The Hill coefficients for the curves that are shown are −1.01 to −0.979. The inset shows the V_{max} value for [^{3}H]dopamine uptake seen after mβCD treatment in percent of control [means ± standard error; $n = 3$, each performed in triplicate; the asterisk indicates a p of <0.05 (t-test)]. (B) Surface biotinylation experiment showing unchanged surface expression of DAT in N2a cells upon treatment with 10 mM mβCD. The surface biotinylation experiments were performed as described in Experimental Procedures. (C) Densitometry analysis of surface biotinylation experiments. Data are the levels of surface expression seen after mβCD treatment in percent of control (means ± standard error; $n = 3$).

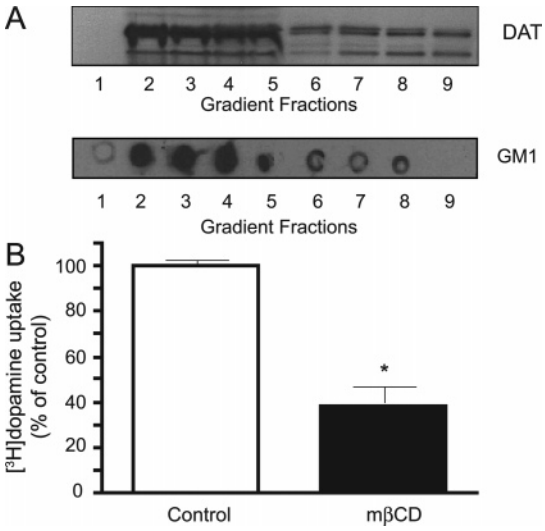

FIGURE 10: Presence of DAT in membrane raft fractions from rat striatal synaptosomes and effect of cholesterol depletion on synaptosomal dopamine uptake. (A) Presence of DAT in membrane raft fractions from rat striatal synaptosomes. Synaptosomes were extracted with 0.4% Triton X-100, and sucrose density gradients were performed. The proteins from fractions 1−9 (from top to bottom) were separated by SDS−PAGE and probed with antibodies against the indicated proteins. DAT proteins are found both in membrane raft fractions (3−5) and in non-membrane raft fractions (7−10). Membrane raft fractions were confirmed by the presence of the membrane raft marker GM1. Representative immunoblots of three independent experiments are shown. (B) DAT activity in striatal synaptosomes with or without pretreatment with 3.75 mM mβCD. Rat striatal synaptosomal preparations were preincubated with mβCD (3.75 mM) for 10 min at 37 °C followed by measurement of the rate of [^{3}H]dopamine uptake. Data are means ± the standard error of the mean ($n = 3$). The asterisk indicates a p of <0.001 compared with the value of the vehicle (two-tailed t-test).

Table 1: Comparison of Diffusion Coefficients Determined by FRAP and FCS in HEK293 Cells[a]

	FRAP D (cm^2/s)	FCS D (cm^2/s)
EGFP-PICK1	$(11.3 \pm 1.8) \times 10^{-9}$	$(12.8 \pm 1.4) \times 10^{-9}$
EGFP-PICK1 with DAT	$(0.44 \pm 0.18) \times 10^{-9}$	$(4.5 \pm 0.05) \times 10^{-9}$
YFP-DAT	$(0.39 \pm 0.08) \times 10^{-9}$	$(3.6 \pm 0.2) \times 10^{-9}$

[a] Diffusion coefficients (D) were determined as described in Experimental Procedures. The resulting D values are given as means ± the standard error of at least five experiments.

from tens of molecules rather than the thousands that are examined using other techniques (*22*, *23*). It is even sensitive enough to detect a single molecule passing through the confocal volume and can provide results detailing a more accurate picture of the movements of a protein over short distances in the cell (approximately 200 nm) (*22*, *23*). In contrast, FRAP data are obtained from a larger sampling area. However, FRAP is generally easier to use than FCS, especially because both the experimental setup and the data analysis are simpler (*21*).

Application of FCS revealed that in HEK-293 cells YFP-tagged DAT is a relatively freely diffusing protein in the plasma membrane with a diffusion coefficient similar to the value recently published for GFP-tagged NET (*24*) as well as to values observed for other membrane proteins using FCS (*35*, *39*, *40*). For EGFP-PICK1, a cytosolic protein that binds to the C-terminus of DAT, binding of EGFP-PICK1 to the DAT not only resulted in recruitment of EGFP-PICK1 to the plasma membrane but also was associated with a marked change in its lateral mobility. This might prove relevant in, for example, high-throughput screening applications; hence, our data show how FCS can provide a rapidly achievable quantitative measure of the interaction between a cytosolic and an integral membrane protein (*41*, *42*).

The lateral mobility of the DAT in the plasma membrane displayed a remarkable dependence on the cellular environment. Specifically, we were unable to assess YFP-DAT diffusion with FCS in N2a cells because of bleaching of the fluorophore. The most reasonable explanation is that YFP-DAT is immobilized or too slowly diffusing in the plasma membrane to allow FCS measurements (Figure 3). Intense bleaching effects have been observed previously for fluorescently labeled cholera toxin on the surface of Vero cells and were interpreted as a population of a relatively immobile protein ($D < 10^{-10}$ cm^2/s or residence times of more than 1 s) (*43*). Partial immobilization of YFP-DAT in N2a cells was supported by application of FRAP. Notably, our ability to detect mobile YFP-DAT in N2a cells with FRAP even when FCS analysis was not achievable likely reflects differences between the two measuring techniques. In FCS, all the fluorescent molecules in the sampling area are tracked. If a significant proportion of these molecules are immobile or moving very slowly, substantial bleaching is unavoidable and will hamper the autocorrelation function. In FRAP, the measurement begins after all molecules in the sampling area

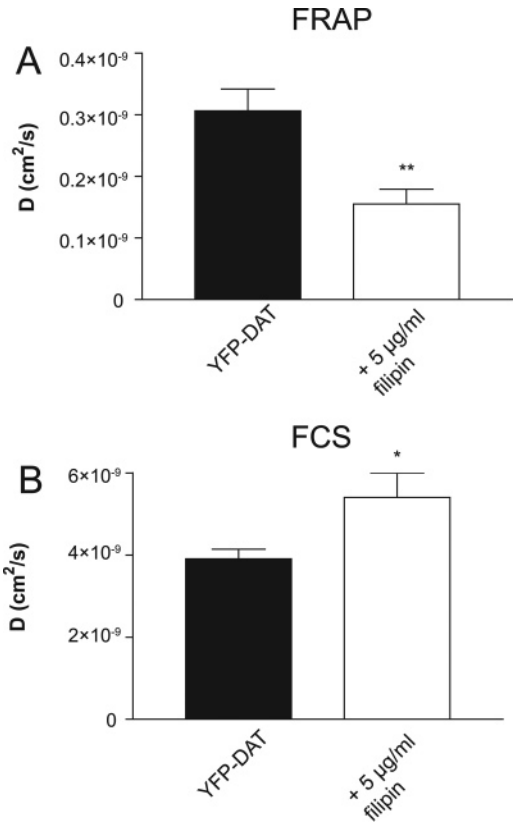

FIGURE 11: Comparison of diffusion coefficients obtained with FCS and FRAP. (A) Diffusion coefficients obtained by FRAP for YFP-DAT in HEK293 cells without and with incubation with 2 μg/mL filipin. (B) Diffusion coefficients obtained by FCS for YFP-DAT in HEK293 cells without and with incubation with 2 μg/mL filipin. Data are means $\pm$ the standard error ($n = 3$). One asterisk indicates a p of <0.05 (t-test), and three asterisks indicate a p of <0.001 (t-test).

have been bleached and the signal results from only mobile molecules moving into this region of interest.

Our FRAP measurements revealed a distinct lateral mobility profile of DAT, in N2a cells in comparison to two other integral membrane proteins, the β2AR, a G protein-coupled receptor, and EGFR, a receptor tyrosine kinase. Most likely, this reflects association of the transporter with the cytoskeleton and/or specific lipid environments since both disruption of the cytoskeleton with cytochalasin D and disruption of membrane rafts by cholesterol depletion with mβCD resulted in a significantly increased rate of lateral diffusion. The ability of cytoskeleton-disrupting agents to enhance membrane mobility has been demonstrated also for other membrane proteins such as the LH receptor and the Na^+/K^+-ATPase (*44*, *45*) and is likely to reflect disruption of a direct or indirect association between the protein of interest and the cytoskeleton (*44*, *45*). The ability of mβCD to enhance membrane mobility might reflect the fact that DAT also associates with membrane rafts. Indeed, we could demonstrate biochemically that the DAT in part associated with the membrane raft fraction in sucrose gradient centrifugation experiments both in N2a cells and in rat brain synaptosomes. However, we should note that the definition of membrane raft association by this type of experiments ("detergent resistance") recently has been subjected to intense scrutiny (*12*). It is, therefore, critical that we provide further support for DAT raft association in a CTB antibody patching experiment in N2a cells (Figure 8).

EGFR is also known to be raft-associated (*46*), and for this protein, we did not see an effect on lateral mobility in response to mβCD. Moreover, it has been argued that on the basis of FRAP experiments membrane raft association is not the dominant factor in determining the long-range protein mobility of membrane proteins at the cell surface (*47*). Thus, the effect of mβCD on DAT lateral mobility might not be a consequence of membrane raft association per se. Instead, it is possible that in the N2a cells raft association could enhance the interaction between the DAT and putative protein complexes in the rafts that represent the determinants of the lateral mobility of the DAT at the plasma membrane.

The suggested membrane raft association of the DAT complements earlier studies showing raft association of the two other biogenic amine transporters, SERT and NET (*18*−*20*). The alteration in DAT transport function with decreases in both V_{max} and K_M, upon treatment of either N2a cells or rat striatal synaptosomes with mβCD, corresponds well with previous data published for the SERT (*18*). Thus, raft association and/or cholesterol might play a role in regulating both SERT and DAT activity. Given the distribution of the DAT in a raft and a nonraft compartment with putative distinct transport properties, we might have expected to observe biphasic kinetics in the uptake experiments: however, both in the presence and in the absence of mβCD, we observed Hill coefficients close to unity. The most likely explanation is that the difference in the K_M values, although significant, still is relatively small, making it difficult to unravel biphasic kinetics. Nevertheless, further studies are required to clarify whether the observed changes in uptake represent a direct or indirect effect on the transporter molecule. It also should be emphasized that the decrease in the rate of uptake and the increase in DAT lateral mobility observed in the N2a cells in response to mβCD are not necessarily direct consequences of the same phenomenon.

The parallel application of FCS and FRAP allowed a direct comparison between the two techniques. Remarkably, whereas D values calculated from either FCS or FRAP were similar for a cytoplasmic protein such as PICK1, the D values obtained for the investigated membrane proteins were approximately 10-fold different (Table 1). We believe that this discrepancy between the D values is likely to reflect inherent differences in what the techniques measure. Indeed, the ability of the raft-disrupting reagent filipin to elicit opposing effects on the rate of diffusion as measured with FCS and FRAP supports the notion that the two methods predominantly measured the DAT in different environments. In this context, it is interesting to note that FCS will select for more rapidly moving protein; i.e., slower moving molecules are likely to be neglected due to photobleaching. An important difference between FCS and FRAP is also that the sampling radii differ between the two methods. We determined the radius of the argon laser beam waist to be 0.19 μm at 514 nm (diameter, 0.38 μm), and the average ROI for FRAP has a radius of 0.98 μm (diameter, 1.96 μm). It is thus possible that whereas FCS may be detecting relatively fast protein movements within a confined domain, FRAP may be detecting long-range diffusion between domains in the membrane. Interestingly, it was proposed on

the basis of the application of vrFRAP (variable observation radius FRAP) that the neurokinin-2 receptor diffuses within confined domains with a mean radius of ~400 nm with a *D* value (1.0×10^{-9} cm^2/s) markedly higher than that observed for long-range diffusion between domains (0.4×10^{-9} cm^2/s) (*48*). Compartmentalization of membrane proteins into confined plasma membrane domains ranging in size from a radius of 100 nm to a radius of 500 nm has also been suggested on the basis of single-molecule tracking techniques for a number of proteins, including the transferrin receptor (*49*), the μ-opioid receptor (*50*), and the human MHC class I protein (*51*). The molecular nature of the confined domains is not entirely clear. They might be the result of long-range attractions between proteins and thus not involve physical fences or direct protein−protein interactions (*50*). Alternatively, they might involve cytoskeletal corrals (*49*). It is also interesting to pay attention to the differential effect of filipin on *D* values determined by either FCS or FRAP, which indirectly could suggest a role of membrane rafts. Addition of filipin results in the clustering of cholesterol moieties in the lipid surface. On a small distance scale, such as that defined by the laser spot in FCS, there is little effect. On a larger distance scale, however, such as that defined by a FRAP region of interest, these cholesterol clusters may create barriers to random walk, thus resulting in a lower diffusion coefficient.

In summary, we have used several techniques to investigate microdomain association of the DAT in different cellular environments. Our data suggest not only that the DAT might associate with both membrane rafts and the cytoskeleton but also that these associations, at least in case of the membrane rafts, might play a role in regulating transporter function. Interestingly, our data also reveal unique lateral diffusion properties of YFP-DAT compared to those of other integral membrane proteins such as the EGFP-β2AR and EGFP-EGFR. Altogether, these distinct lateral diffusion profiles for three distinct membrane proteins in two different cell lines underline the importance of critically evaluating the cellular context when studying the function and regulation of these types of proteins.

ACKNOWLEDGMENT

We thank Drs. Petra Schwille and Bo van Deurs for helpful advice.

REFERENCES

1. Torres, G. E., Gainetdinov, R. R., and Caron, M. G. (2003) Plasma membrane monoamine transporters: Structure, regulation and function, *Nat. Rev. Neurosci. 4*, 13−25.
2. Chen, N. H., Reith, M. E., and Quick, M. W. (2004) Synaptic uptake and beyond: The sodium- and chloride-dependent neurotransmitter transporter family SLC6, *Pfluegers Arch. 447*, 519−531.
3. Gether, U., Andersen, P. H., Larsson, O. M., and Schousboe, A. (2006) Neurotransmitter transporters: Molecular function of important drug targets, *Trends Pharmacol. Sci. 27*, 375−383.
4. Yamashita, A., Singh, S. K., Kawate, T., Jin, Y., and Gouaux, E. (2005) Crystal structure of a bacterial homologue of Na^+/Cl^--dependent neurotransmitter transporters, *Nature 437*, 215−223.
5. Goldberg, N. R., Beuming, T., Soyer, O. S., Goldstein, R. A., Weinstein, H., and Javitch, J. A. (2003) Probing conformational changes in neurotransmitter transporters: A structural context, *Eur. J. Pharmacol. 479*, 3−12.
6. Rudnick, G. (2006) Structure/function relationships in serotonin transporter: New insights from the structure of a bacterial transporter, *Handb. Exp. Pharmacol. 175*, 59−73.
7. Carneiro, A. M., Ingram, S. L., Beaulieu, J. M., Sweeney, A., Amara, S. G., Thomas, S. M., Caron, M. G., and Torres, G. E. (2002) The multiple LIM domain-containing adaptor protein Hic-5 synaptically colocalizes and interacts with the dopamine transporter, *J. Neurosci. 22*, 7045−7054.
8. Lee, K. H., Kim, M. Y., Kim, D. H., and Lee, Y. S. (2004) Syntaxin 1A and receptor for activated C kinase interact with the N-terminal region of human dopamine transporter, *Neurochem. Res. 29*, 1405−1409.
9. Torres, G. E., Yao, W. D., Mohn, A. R., Quan, H., Kim, K. M., Levey, A. I., Staudinger, J., and Caron, M. G. (2001) Functional interaction between monoamine plasma membrane transporters and the synaptic PDZ domain-containing protein PICK1, *Neuron 30*, 121−134.
10. Bjerggaard, C., Fog, J., Hastrup, H., Madsen, K., Javitch, J. A., and Gether, U. (2004) Surface targeting of the dopamine transporter involves discrete epitopes in the distal carboxyterminus but occurs independently of canonical PDZ domain interactions, *J. Neurosci. 24*, 7024−7036.
11. Fog, J. U., Khoshbouei, H., Holy, M., Owens, W. A., Vaegter, C. B., Sen, N., Nikandrova, Y., Bowton, E., McMahon, D. G., Colbran, R. J., Daws, L. C., Sitte, H. H., Javitch, J. A., Galli, A., and Gether, U. (2006) Calmodulin Kinase II Interacts with the Dopamine Transporter C Terminus to Regulate Amphetamine-Induced Reverse Transport, *Neuron 51*, 417−429.
12. Pike, L. J. (2006) Rafts defined: A report on the Keystone Symposium on Lipid Rafts and Cell Function, *J. Lipid Res. 47*, 1597−1598.
13. Simons, K., and Toomre, D. (2000) Lipid rafts and signal transduction, *Nat. Rev. Mol. Cell Biol. 1*, 31−39.
14. Tsui-Pierchala, B. A., Encinas, M., Milbrandt, J., and Johnson, E. M., Jr. (2002) Lipid rafts in neuronal signaling and function, *Trends Neurosci. 25*, 412−417.
15. Chini, B., and Parenti, M. (2004) G-Protein coupled receptors in lipid rafts and caveolae: How, when and why do they go there? *J. Mol. Endocrinol. 32*, 325−338.
16. Monastyrskaya, K., Hostettler, A., Buergi, S., and Draeger, A. (2005) The NK1 receptor localizes to the plasma membrane microdomains, and its activation is dependent on lipid raft integrity, *J. Biol. Chem. 280*, 7135−7146.
17. Butchbach, M. E., Tian, G., Guo, H., and Lin, C. L. (2004) Association of excitatory amino acid transporters, especially EAAT2, with cholesterol-rich lipid raft microdomains: Importance for excitatory amino acid transporter localization and function, *J. Biol. Chem. 279*, 34388−34396.
18. Magnani, F., Tate, C. G., Wynne, S., Williams, C., and Haase, J. (2004) Partitioning of the serotonin transporter into lipid microdomains modulates transport of serotonin, *J. Biol. Chem. 279*, 38770−38778.
19. Samuvel, D. J., Jayanthi, L. D., Bhat, N. R., and Ramamoorthy, S. (2005) A role for p38 mitogen-activated protein kinase in the regulation of the serotonin transporter: Evidence for distinct cellular mechanisms involved in transporter surface expression, *J. Neurosci. 25*, 29−41.
20. Jayanthi, L. D., Samuvel, D. J., and Ramamoorthy, S. (2004) Regulated internalization and phosphorylation of the native norepinephrine transporter in response to phorbol esters. Evidence for localization in lipid rafts and lipid raft-mediated internalization, *J. Biol. Chem. 279*, 19315−19326.
21. Day, R. N., and Schaufele, F. (2005) Imaging molecular interactions in living cells, *Mol. Endocrinol. 19*, 1675−1686.
22. Gosch, M., and Rigler, R. (2005) Fluorescence correlation spectroscopy of molecular motions and kinetics, *Adv. Drug Delivery Rev. 57*, 169−190.
23. Haustein, E., and Schwille, P. (2004) Single-molecule spectroscopic methods, *Curr. Opin. Struct. Biol. 14*, 531−540.
24. Schwartz, J. W., Novarino, G., Piston, D. W., and DeFelice, L. J. (2005) Substrate binding stoichiometry and kinetics of the norepinephrine transporter, *J. Biol. Chem. 280*, 19177−19184.
25. Axelrod, D., Koppel, D. E., Schlessinger, J., Elson, E., and Webb, W. W. (1976) Mobility measurement by analysis of fluorescence photobleaching recovery kinetics, *Biophys. J. 16*, 1055−1069.
26. Rees, S., Coote, J., Stables, J., Goodson, S., Harris, S., and Lee, M. G. (1996) Bicistronic vector for the creation of stable mammalian cell lines that predisposes all antibiotic-resistant cells to express recombinant protein, *BioTechniques 20*, 102−110.

27. Saunders, C., Ferrer, J. V., Shi, L., Chen, J., Merrill, G., Lamb, M. E., Leeb-Lundberg, L. M., Carvelli, L., Javitch, J. A., and Galli, A. (2000) Amphetamine-induced loss of human dopamine transporter activity: An internalization-dependent and cocaine-sensitive mechanism, *Proc. Natl. Acad. Sci. U.S.A. 97*, 6850−6855.
28. Yguerabide, J., Schmidt, J. A., and Yguerabide, E. E. (1982) Lateral mobility in membranes as detected by fluorescence recovery after photobleaching, *Biophys. J. 40*, 69−75.
29. Becher, A., White, J. H., and McIlhinney, R. A. (2001) The γ-aminobutyric acid receptor B, but not the metabotropic glutamate receptor type-1, associates with lipid rafts in the rat cerebellum, *J. Neurochem. 79*, 787−795.
30. Chmelar, R. S., and Nathanson, N. M. (2006) Identification of a novel apical sorting motif and mechanism of targeting of the M2 muscarinic acetylcholine receptor, *J. Biol. Chem. 281*, 35381−35396.
31. Kahlig, K. M., Javitch, J. A., and Galli, A. (2004) Amphetamine regulation of dopamine transport. Combined measurements of transporter currents and transporter imaging support the endocytosis of an active carrier, *J. Biol. Chem. 279*, 8966−8975.
32. Haupts, U., Maiti, S., Schwille, P., and Webb, W. W. (1998) Dynamics of fluorescence fluctuations in green fluorescent protein observed by fluorescence correlation spectroscopy, *Proc. Natl. Acad. Sci. U.S.A. 95*, 13573−13578.
33. Schwille, P., Kummer, S., Heikal, A. A., Moerner, W. E., and Webb, W. W. (2000) Fluorescence correlation spectroscopy reveals fast optical excitation-driven intramolecular dynamics of yellow fluorescent proteins, *Proc. Natl. Acad. Sci. U.S.A. 97*, 151−156.
34. Lippincott-Schwartz, J., Snapp, E., and Kenworthy, A. (2001) Studying protein dynamics in living cells, *Nat. Rev. Mol. Cell Biol. 2*, 444−456.
35. Brock, R., Hamelers, I. H., and Jovin, T. M. (1999) Comparison of fixation protocols for adherent cultured cells applied to a GFP fusion protein of the epidermal growth factor receptor, *Cytometry 35*, 353−362.
36. Bacia, K., Scherfeld, D., Kahya, N., and Schwille, P. (2004) Fluorescence correlation spectroscopy relates rafts in model and native membranes, *Biophys. J. 87*, 1034−1043.
37. Janes, P. W., Ley, S. C., and Magee, A. I. (1999) Aggregation of lipid rafts accompanies signaling via the T cell antigen receptor, *J. Cell Biol. 147*, 447−461.
38. Boesze-Battaglia, K. (2006) Isolation of membrane rafts and signaling complexes, *Methods Mol. Biol. 332*, 169−179.
39. Hegener, O., Prenner, L., Runkel, F., Baader, S. L., Kappler, J., and Haberlein, H. (2004) Dynamics of β2-adrenergic receptor-ligand complexes on living cells, *Biochemistry 43*, 6190−6199.
40. Meissner, O., and Haberlein, H. (2003) Lateral mobility and specific binding to GABA(A) receptors on hippocampal neurons monitored by fluorescence correlation spectroscopy, *Biochemistry 42*, 1667−1672.
41. Maertens, G., Vercammen, J., Debyser, Z., and Engelborghs, Y. (2005) Measuring protein-protein interactions inside living cells using single color fluorescence correlation spectroscopy. Application to human immunodeficiency virus type 1 integrase and LEDGF/p75, *FASEB J. 19*, 1039−1041.
42. Brock, R., Vamosi, G., Vereb, G., and Jovin, T. M. (1999) Rapid characterization of green fluorescent protein fusion proteins on the molecular and cellular level by fluorescence correlation microscopy, *Proc. Natl. Acad. Sci. U.S.A. 96*, 10123−10128.
43. Bacia, K., Majoul, I. V., and Schwille, P. (2002) Probing the endocytic pathway in live cells using dual-color fluorescence cross-correlation analysis, *Biophys. J. 83*, 1184−1193.
44. Roess, D. A., Niswender, G. D., and Barisas, B. G. (1988) Cytochalasins and colchicine increase the lateral mobility of human chorionic gonadotropin-occupied luteinizing hormone receptors on ovine luteal cells, *Endocrinology 122*, 261−269.
45. Paller, M. S. (1994) Lateral mobility of Na,K-ATPase and membrane lipids in renal cells. Importance of cytoskeletal integrity, *J. Membr. Biol. 142*, 127−135.
46. Roepstorff, K., Thomsen, P., Sandvig, K., and van Deurs, B. (2002) Sequestration of epidermal growth factor receptors in non-caveolar lipid rafts inhibits ligand binding, *J. Biol. Chem. 277*, 18954−18960.
47. Kenworthy, A. K., Nichols, B. J., Remmert, C. L., Hendrix, G. M., Kumar, M., Zimmerberg, J., and Lippincott-Schwartz, J. (2004) Dynamics of putative raft-associated proteins at the cell surface, *J. Cell Biol. 165*, 735−746.
48. Cezanne, L., Lecat, S., Lagane, B., Millot, C., Vollmer, J. Y., Matthes, H., Galzi, J. L., and Lopez, A. (2004) Dynamic confinement of NK2 receptors in the plasma membrane. Improved FRAP analysis and biological relevance, *J. Biol. Chem. 279*, 45057−45067.
49. Sako, Y., and Kusumi, A. (1994) Compartmentalized structure of the plasma membrane for receptor movements as revealed by a nanometer-level motion analysis, *J. Cell Biol. 125*, 1251−1264.
50. Daumas, F., Destainville, N., Millot, C., Lopez, A., Dean, D., and Salome, L. (2003) Confined diffusion without fences of a g-protein-coupled receptor as revealed by single particle tracking, *Biophys. J. 84*, 356−366.
51. Smith, P. R., Morrison, I. E., Wilson, K. M., Fernandez, N., and Cherry, R. J. (1999) Anomalous diffusion of major histocompatibility complex class I molecules on HeLa cells determined by single particle tracking, *Biophys. J. 76*, 3331−3344.

BI700429Z